INL/CON-10-20731
PREPRINT

Scale Analysis of Convective Melting with Internal Heat Generation

AJTEC 2011

Ali Siahpush
John Crepeau

March 2011

The INL is a
U.S. Department of Energy
National Laboratory
operated by
Battelle Energy Alliance

Proceedings of the ASME/JSME 8th Thermal Engineering Joint Conference
AJTEC2011
March 13-17, 2011, Honolulu, Hawaii, USA

AJTEC2011-44162

SCALE ANALYSIS OF CONVECTIVE MELTING WITH INTERNAL HEAT GENERATION

Ali Siahpush
Idaho National Laboratory
Idaho Falls, Idaho, USA

John Crepeau
University of Idaho
Moscow, Idaho, USA

ABSTRACT

Using a scale analysis approach, we model phase change (melting) for pure materials which generate internal heat for small Stefan numbers (approximately one). The analysis considers conduction in the solid phase and natural convection, driven by internal heat generation, in the liquid regime. The model is applied for a constant surface temperature boundary condition where the melting temperature is greater than the surface temperature in a cylindrical geometry. We show the time scales in which conduction and convection heat transfer dominate.

NOMENCLATURE

c_p – specific heat (kJ/kg K)
g –gravitational constant (m/s^2)
Δh_f – Latent heat (kJ/kg)
H – height of cylinder (m)
k – thermal conductivity (W/m K)
$\dot{q}$ - internal heat generation (W/m^3)
r – radial distance (m)
Ra_H – Rayleigh number ($\rho\beta g \dot{q} H^5/\mu\alpha k$)
Ra_z – Rayleigh number ($\rho\beta g \dot{q} z^5/\mu\alpha k$)
s – distance from CL to phase front (m)
St – Stefan number ($c_p\Delta T/\Delta h$)
t – time (s)
T – temperature (K)
T_m – melting temperature (K)
u, v, w – velocity components (m/s)
x, y, z – spatial components (m)

Greek
α – thermal diffusivity (m^2/s)
β – coefficient of thermal expansion (1/K)
δ_z – thermal boundary layer thickness (m)
μ – dynamic viscosity (kg m/s)
ν – kinematic viscosity (m^2/s)
ρ - density (kg/m^3)
θ – nondimensional time, ($\dot{q}$ /$\rho\Delta h_f$)

Subscripts
A,B,C,D – regime designations
CL – centerline
f - fusion
l – liquid
s – solid
0 – initial value
∞ - freestream

INTRODUCTION

Solid-liquid phase change driven by internal heat generation is a phenomenon encountered in many physical systems including geophysics, cryosurgery and materials processing among others. It is also encountered in nuclear systems, primarily in fuel rods during accident scenarios. The nonhomogeneous heat generation term in the energy equation makes an exact solution difficult to find. Complicating the solution is convection in the liquid phase of the material. Viskanta [1] has reviewed the literature regarding natural convection in melting and solidification processes. Early analytical studies on free

convection driven by internal heat generation with no phase change in a vertical cylinder were performed by Martin [2]. He used the integral method to find temperature and velocity profiles within the cylinder. Vajravelu [3] studied natural convection driven by internal heat generation in a fluid on the surface of a heated semi-infinite vertical plate. He found that the heat sources considerably increased the temperature and velocity fields. Daniels and Jones [4] used the method of matched asymptotic expansions to find steady two-dimensional motion generated in a shallow cavity by uniformly distributed internal heat sources. Their solutions showed how the Rayleigh number influences the shape and speeds of the convection cells formed in the shallow rectangular cavity. Tasaka et al. [5] investigated experimentally natural convection induced by internal heat generation, showing that the convection cells dilate with increasing Rayleigh number. They used thermochromic liquid crystals to visualize the motion of the convection cells. The temperature profiles show that the high temperature areas within the cell occur at the apexes. An analytical study for natural convection in a cavity of different aspect ratios with a uniform volumetric heat generation was performed by Joshi et al. [6]. They found that the horizontal component of the velocity is smaller than the vertical component near the center and walls of the cavity. They compared their results to computational results showing good agreement. Approximate solutions of phase change with natural convection were studied by Tien and Yen [7]. They found good comparisons of their analytical solutions to numerical ones for water-ice systems.

The method used in this paper to study phase change and natural convection with internal heat generation is the scale analysis technique introduced by Bejan [8]. The scale analysis method finds order-of-magnitude estimates to get an idea of the behavior for physical systems. This method has also been used and described by Astarita [9] to gain significant physical insight to various problems. Zhang and Bejan [10] used scale analysis to study time-dependent natural convection melting with conduction in the solid. They found that in the conduction dominated regime, the Nusselt number increases as the solid subcooling parameter increases. Scale analysis was also used to study turbulent heat transfer driven by buoyancy in a porous layer with homogeneous heat sources by Kim and Kim [11]. They found a critical Rayleigh number for the onset of natural convection.

In this paper, we model natural convection driven by internal heat generation in the presence of internal heat generation. This is an extension to numerical work published previously [12].

SCALE ANALYSIS

We begin our two-dimensional, steady-state scale analysis in cylindrical coordinates, using the conservation of mass, momentum and energy equations [13],

$$\frac{\partial u}{\partial r}+\frac{\partial w}{\partial z}=0 \tag{1}$$

$$u\frac{\partial w}{\partial r}+w\frac{\partial w}{\partial z}=-g\beta\Delta T+\nu\left(\frac{\partial^2 w}{\partial r^2}+\frac{1}{r}\frac{\partial w}{\partial r}+\frac{\partial^2 w}{\partial z^2}\right) \tag{2}$$

$$u\frac{\partial T}{\partial r}+w\frac{\partial T}{\partial z}=\frac{\dot{q}}{\rho c_p}+\alpha\left(\frac{\partial^2 T}{\partial r^2}+\frac{1}{r}\frac{\partial T}{\partial r}+\frac{\partial^2 T}{\partial z^2}\right) \tag{3}$$

We have assumed that the heat transfer is axisymmetric. In Eq. (2), the Boussinesq Approximation has been used to eliminate the pressure term and have it replaced with the buoyancy term. Figure 1 shows a schematic of the geometry.

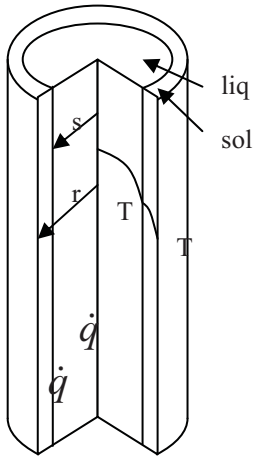

Figure 1. Schematic diagram of phase change in a cylinder with volumetric heat generation

REGIME ANALYSIS

Regime A

To start the scale analysis, we begin first with a cylindrical material which generates internal heat. The radius of the cylinder is r_0, and the surface of the cylinder is kept a constant temperature, $T_0 < T_m$. Since the material generates internal heat, the temperature profile within the material is parabolic with its maximum at the centerline [13]. If the internal heat generation is large enough, the material first begins to melt along the centerline. Figure 2 gives a schematic of material during Regime A.

We first consider the case where a thin layer of material just starts to melt along the centerline, and in this early part of the melting process, there is no convection in the liquid. The melting temperature of the material is T_m, and the temperature in the liquid is assumed to be constant at the melting temperature.

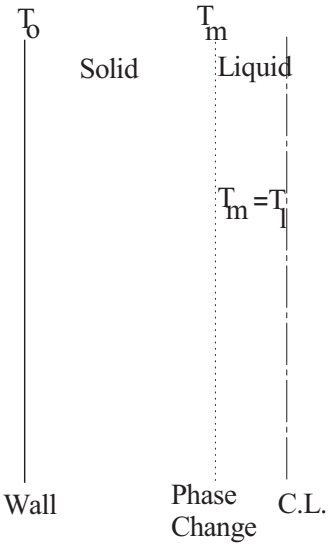

Figure 2. Schematic diagram of Regime A.

In general, along the solid-liquid interface [14],

$$k_l \frac{dT_l}{dr} + \rho_s \Delta h_s \frac{ds}{dt} = k_s \frac{dT_s}{dr} \tag{4}$$

For a constant temperature in the liquid (no heat transfer occurs since $T_0 = T_m$), Eq. (4) becomes,

$$\rho_s \Delta h_f \frac{ds}{dt} = k_s \frac{dT_s}{dr} \tag{5}$$

From Crepeau and Siahpush [15], the slope of the temperature profile within the solid region is,

$$\left.\frac{dT_s}{dr}\right|_{r=s} = -\frac{\dot{q}s}{2k_s} + \frac{\left(s^2 - r_0^2\right)\dot{q} + 4k_s\left(T_m - T_0\right)}{4k_s s\left(\ln s - \ln r_0\right)} \tag{6}$$

Substituting Eq. (6) into Eq. (5) and reducing gives,

$$\frac{ds}{dt} = -\frac{\dot{q}s}{2\rho_s \Delta h_f} + \frac{\left(s^2 - r_0^2\right)\dot{q}}{4s\ln\left(s/r_0\right)\rho_s \Delta h_f} + \frac{\alpha St_s}{s\ln\left(s/r_0\right)} \tag{7}$$

We now perform a scale analysis in cylindrical coordinates [8], comparing relative sizes of the terms in Eq. (7). The scaled form of Eq. (7) becomes,

$$\frac{s}{t} \sim \frac{\dot{q}s}{\rho_s \Delta h_f}, \frac{\left(s^2 - r_0^2\right)\dot{q}}{s\ln\left(s/r_0\right)\rho_s \Delta h_f}, \frac{\alpha_s St_s}{s\ln\left(s/r_0\right)} \tag{8}$$

Since the diameter of the melted region is small compared to the radius, $s \ll r_0$, (terms having $\ln(s/r_0)$ are small) we find,

$$t_A \sim \frac{\rho_s \Delta h_f}{\dot{q}} \tag{9}$$

At t_A, Regime A disappears. In this regime, the thickness of the liquid is small and in a very short period of time, the temperature of the thin layer of liquid will be above the melting point of the material. At this point, heat transfer in the liquid begins.

Regime B

In this regime, the melted portion has grown, but heat transfers only by conduction in both the solid and liquid regions. The liquid layer remains relatively thin. Figure 3 shows Regime B.

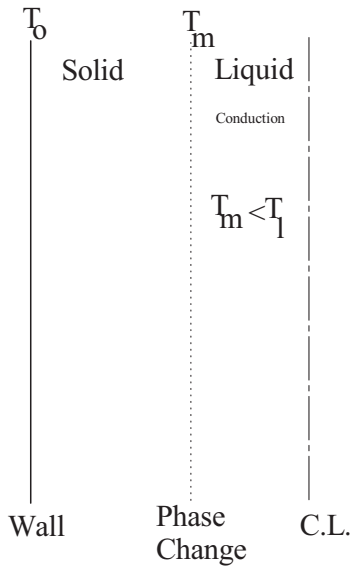

Figure 3. Schematic of Regime B.

For $s^2 \ll r_0^2$, the interface equation, Eq. (7), scales as,

$$\frac{s^2}{t} \sim \frac{r_0^2 \dot{q}}{\rho_s \Delta h_f \ln\left(s/r_0\right)}, \frac{\alpha St_l}{\ln\left(s/r_0\right)} \tag{10}$$

For small Stefan numbers and $\ln\left(s/r_0\right) \sim 1$, the distance to the phase change interface, s, becomes,

$$s^2 \sim \frac{r_0^2 \dot{q}}{\rho_s \Delta h_f} t \tag{11}$$

The nondimensional time is then defined as,

$$\theta = \frac{\dot{q}}{\rho \Delta h_f} t \tag{12}$$

So,

$$s \sim r_0 \theta^{1/2} \tag{13}$$

Regime C

In the previous regime, heat transferred solely by conduction in both the liquid and solid phases. Regime C begins when convection starts in the liquid portion of the melt. Figure 4 shows the state of the system during Regime C. Experimental evidence [16] shows that convection in the liquid begins along the top portion of the cylinder and along the bottom of the cylinder, heat transfers by conduction. It should be noted that in the convection upper zone, the thermal boundary layer thickness (δ_z) is of the same order of magnitude as the gap thickness of the lower conduction zone (s) and the liquid thickness, $\delta_z = s$.

We can scale the terms in Eqs. (1-3), the conservation of mass, momentum and energy, respectively, in the following way,

$$\begin{aligned} &\frac{u}{s} \sim \frac{w}{H} \\ &\frac{w^2}{H} \sim \beta g \Delta T_l, \nu \frac{w}{s^2} \\ &\frac{w}{H}\Delta T_l, \frac{\dot{q}}{\rho c_p} \sim \alpha \frac{\Delta T_l}{s^2} \end{aligned} \tag{14}$$

All of the properties in Eq. (14) are for the liquid phase. For conduction in the liquid,

$$\frac{w}{H}\Delta T_l \ll \alpha \frac{\Delta T_l}{s^2} \tag{15}$$

The scaled energy equation then reduces to,

$$\frac{\dot{q}}{\rho c_p} \sim \alpha \frac{\Delta T_l}{s^2} \tag{16}$$

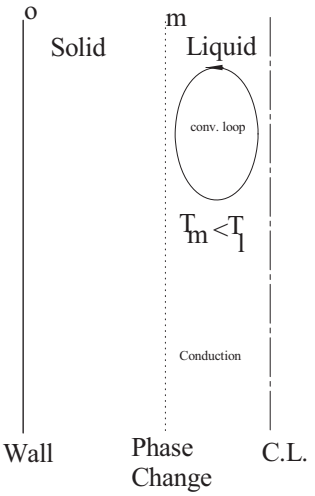

Figure 4. State of the system during Regime C.

In the upper portion under steady-state conditions, we get,

$$\frac{w^2}{H} \to 0, \quad \alpha \frac{\Delta T_l}{s^2} \to 0 \tag{17}$$

The term w^2/H goes to zero since the velocity in the z-direction is small compared to H. The governing equations become,

$$\begin{aligned} &\frac{u}{\delta_z} \sim \frac{w}{H} \\ &\beta g \Delta T_l \sim \nu \frac{w}{\delta_z^2} \\ &\frac{w}{H}\Delta T_l \sim \frac{\dot{q}}{\rho c_p} \end{aligned} \tag{18}$$

For a Rayleigh number defined for convection driven by internal heat generation, [17]

$$Ra_H = \frac{\rho \beta g \dot{q} H^5}{\mu \alpha k}, \quad Ra_z = \frac{\rho \beta g \dot{q} z^5}{\mu \alpha k} \tag{19}$$

The height of the upper convection zone is given by z. When $z = H$, convection heat transfer then dominates in the liquid phase. And taking a ratio between the two,

$$Ra_z = \left(\frac{z}{H}\right)^5 Ra_H \tag{20}$$

Regime C ends when $z = H$. Note that Eq. (13) will give the same value for s since in the convection in the upper zone, the thermal boundary layer thickness (δ_z) is of the same order of magnitude as the gap thickness of the lower conduction zone (s).

From Eq. (13) and the scale of the z-momentum equation, Eq. (18), the scale of the velocity in the z-direction becomes,

$$w \sim \frac{\beta g \Delta T_l}{\nu} \delta_z^2 \tag{21}$$

Substituting into the scaled energy equation,

$$\frac{\beta g}{\nu} \frac{1}{z} \left(\Delta T_l\right)^2 \delta_z^2 \sim \frac{\dot{q}}{\rho c_p} \tag{22}$$

From Martin [17],

$$\Delta T_l = \frac{\nu \alpha H}{\beta g \delta_z^4} \tag{23}$$

Substituting in Eq. (22) and reducing, we find,

$$\delta_z \sim \left(\frac{1}{Ra_z}\right)^{1/6} z \tag{24}$$

If s → δ_z, and z → H, substituting Eq. (24) into Eq. (13) and rearranging terms, we get the non-dimensional time,

$$\theta^{1/2} \sim \left(\frac{1}{Ra_H}\right)^{1/6} \frac{H}{r_0} \tag{25}$$

Inserting from Eq. (12), we get the time where Regime C ends,

$$t_C \sim \frac{\rho \Delta h_f}{\dot{q}} \left[\left(\frac{1}{Ra_H}\right)^{1/6} \frac{H}{r_0}\right]^2 \tag{26}$$

Regime D

In the final regime, the convection that began in the upper portion of the cylinder has now expanded to include the liquid throughout the cylinder. As before, heat transfers solely by conduction in the solid phase. Figure 5 gives the schematic of Regime D.

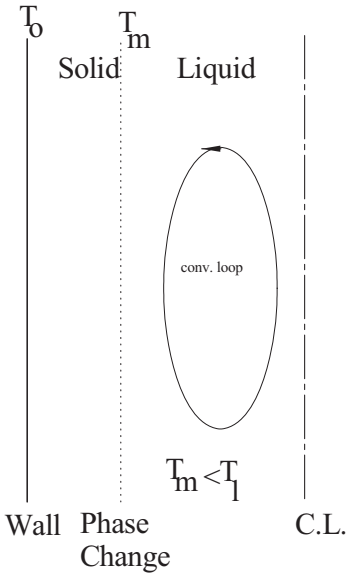

Figure 5. Schematic of Regime D.

We start with the solid-liquid interface equation Eq. (4), and the temperature gradient within the solid phase, Eq. (6) so that the scales of the governing equations become as Eq. (18), with δ_z replaced by the distance to the phase change front *s*,

$$\frac{w}{H}\Delta T_l \sim \frac{\dot{q}}{\rho_l c_{p,l}} \tag{27}$$

$$\beta g \Delta T_l \sim \nu_l \frac{w}{s^2}$$

Substituting and rearranging into the scaled form of the energy equation gives,

$$\frac{\beta g s^2}{\nu_l H}\left(\Delta T_l\right)^2 \sim \frac{\dot{q}}{\rho_l c_{p,l}} \tag{28}$$

From [17],

$$\Delta T_l = T_{CL} - T_m = \left.\frac{\nu_l \alpha_l H}{\beta g s^4}\right|_{liq} \tag{29}$$

Substituting Eq. (29) into Eq. (28), we obtain,

$$\frac{\beta g s^2}{\nu_l H}\left(\frac{\nu \alpha H}{\beta g \dot{q}}\right)^2 \sim \frac{\dot{q}}{\rho_l c_{p,l}} \tag{30}$$

Solving for *s* and inserting the definition of the Rayleigh number Eq. (19), we get,

$$s \sim \left(\frac{1}{Ra_H}\right)^{1/6} H \tag{31}$$

This compares to Eq. (24) when $z = H$, and at this point convection occurs completely throughout the liquid. At this value of *s*, Regime D begins.

By introducing the following nondimensional variables,

$$\tilde{s} = \frac{s}{r_0}, \quad \tau = \frac{\alpha_s}{r_0^2} t, \quad \tilde{r}_s = \frac{r_s}{r_0}$$
$$\tilde{T}_s = \frac{T_m - T_s}{T_m - T_0}, \quad \tilde{T}_l = \frac{T_{CL} - T_s}{T_m - T_0} \tag{32}$$

The interface equation, (Eq. (4)) becomes,

$$\frac{1}{2} Nu_D \tilde{T}_l + \frac{1}{St_l}\frac{d\tilde{s}}{d\tau} = -\frac{dT_s}{d\tilde{r}_s} \tag{33}$$

Equation (33) can be solved numerically to evaluate $\tilde{s}$ at a given time, τ.

RESULTS AND APPLICATION

We then wish to apply the scale analysis given above to the case of the melting problem of UO_2. El-Genk and Cronenberg [18] gave the properties of UO_2 which are used in this scale analysis and are listed in Table 1.

Figure 6 shows the results of the scale analysis for UO_2. In Regime A, the material just starts to melt along the centerline and in this early part of the melting process, there is no convection in the liquid and the temperature in the liquid is assumed to be constant at the melting temperature. The thickness of the liquid is very small and in very short period of time, the temperature of thin layer of liquid will be above melting point of the material and Regime B starts. Equation 9 indicates that Regime A ends at approximately 4 seconds.

Table 1. UO_2 properties

Melt temperature	T_m = 2877°C
Heat of fusion	Δh_f = 65.543 cal/gm
Specific heat of solid	c_{ps}= 0.579 cal/gm°C
Specific heat of liquid	c_{pl} = 0.1194 cal/gm°C
Thermal conductivity of liquid	$k_l = 5.97 \times 10^{-3}$ cal/cm°C sec
Thermal conductivity of solid	$k_s = 5.97 \times 10^{-3}$ cal/cm°C sec
Density of solid	ρ_s=10530 kg/m^3
Density of liquid	ρ_l=8811 kg/m^3
Viscosity	$\mu = 0.988 \times 10^{-2}$ exp(4620/(T+273)) gm/cm sec
Volumetric internal heat generation	Q_{vol}=2.15 cal/cm^{3}sec

For our geometry, we used:

H = 0.5 m
r_o=0.1 m

In Regime B, the melting process is governed strictly by conduction heat transfer in both liquid and solid phases. The heat transfer across the very thin liquid film is absorbed by the latent heat of fusion at the solid-liquid interface. The conduction regime disappears in a relatively short time after the beginning of the experiment. From Eq. 16, we can evaluate the melt thickness or fusion radius. For UO_2, this regime end at approximately 34 seconds.

Regime C begins when convection starts in the liquid portion of the melt and at the interface, the convection heat transfer rate balances the rate at which latent heat is released from the interface. Experimental evidence [16] shows that convection begins along the top portion of the cylinder. Regime C ends when z = H. Equation (25) shows that this regime ends at 34 seconds which coincides with the end of Regime B.

Regime D begins once the transition/mixed regime ends and the quasi-steady convection zone fills the entire liquid space of height *H*. In this regime, the heat transfer and location of the melting front are controlled by the convection contribution. The conduction in liquid is much smaller than the convection and it will disappear. Equation (7) was used to get the portion of the curve for Regime D in Figure 6. This regime ends at 425 seconds and all the material is in liquid phase.

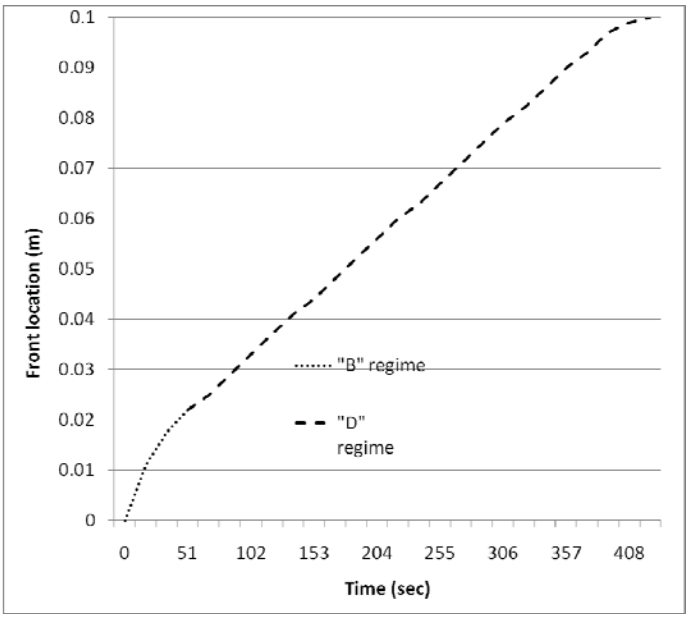

Figure 6. Plot of Regimes A, B, C, and D for the melting of UO_2.

CONCLUSIONS

The object of scale analysis is to use the basic principles of convection heat transfer in order to produce order-of-magnitude estimates for quantities of interest (in our case radius of fusion). When used in conjunction with experimental data, the scale analysis can also be used as a framework for the development of correlations, relating the independent and dependent variables associated with the phenomena. The key to the correct correlation of natural convection melting is the identification of the proper scales of the phenomena in order to construct appropriate correlations for the heat transfer and the melting rate.

Using this method, we model phase change (melting) for materials which generate internal heat for small Stefan numbers (approximately one). The analysis considers conduction in the solid phase and natural convection, driven by internal heat generation, in the liquid regime. The model is applied for a small Stefan number with constant surface temperature boundary condition in a cylindrical geometry.

We identified four different melting regimes and demonstrated the time scales in which conduction and convection heat transfer dominate. For high values of volumetric heat generation rate, after short period of time, convection in liquid dominates the heat transfer mode.

REFERENCES

[1] Viskanta, R. (1985) "Natural Convection in Melting and Solidification," in Natural Convection, Fundamentals and

Applications, eds. S. Kakac, W. Aung, and R. Viskanta, Hemisphere, Washington, DC., pp. 845-877.
[2] Martin, B.W., (1967) “Free convection in a vertical cylinder with internal heat generation,” Proc. Royal Society B, 301, pp. 327-341.
[3] Vajrevelu, R., (1979) “Natural Convection at a heated semiinfinite vertical plate with internal heat generation,” Acta Mechanica, 34, pp. 153-159.
[4] Daniels, P.G., and O.K. Jones, (1998) “Convection in a shallow rectangular cavity due to internal heat generation,” International Journal of Heat and Mass Transfer, 41, pp. 3979-3987.
[5] Tasaka, Y., Y. Kudoh, Y. Takeda, T. Yanagisawa, (2005), “Experimental investigation of natural convection induced by internal heat generation,” Journal of Physics:Conference Series, 14, pp. 168-179.
[6] Joshi, M.V., U.N. Gaitonde, S.K. Mitra, (2006) “Analytical Study of Natural Convection in a Cavity with volumetric heat generation,” J. Heat Transfer, 128, pp. 176-182.
[7] Tien, C. and Y.-C. Yen, (1966) “Approximate solution of a melting problem with natural convection,” AICHE J. 62, pp. 166-172.
[8] Bejan, A., (2004) Convection Heat Transfer, Wiley, New York, 3rd ed.
[9] Astarita, G. (1997) “Dimensional Analysis, scaling, and orders of magnitude,” Chemical Engineering Science, 52, pp. 4681-4698.
[10] Zhang, A. and A. Bejan, (1989) “The problem of time-dependent natural convection melting with conduction in the solid,” Int. J. Heat Mass Trans. (32) pp. 2447-2457.
[11] Kim, S., and M.C. Kim, (2002) “A scale analysis of turbulent heat transfer driven by buoyancy in a porous layer with homogeneous heat sources,” Int. Comm. Heat Mass Trans. 29, pp. 127-134.
[12] Crepeau, J. A. Siahpush and B. Spotten (2009) “On the Stefan Problem with Volumetric Energy Generation,” Heat Mass Transfer, 46, pp. 119-128.
[13] Incropera, F.P., and D.P. DeWitt, (2001), Fundamentals of Heat Transfer, 4th ed. Wiley, New York.
[14] Poulikakos, D., Conduction Heat Transfer, Prentice Hall, Englewood Cliffs.
[15] Crepeau, J.C., and A. Siahpush, (2008), Approximate Solutions to the Stefan Problem with Internal Heat Generation, Heat and Mass Transfer, 44, pp. 787-794.
[16] Siahpush, A., (2002) Performance Enhancement of Solid/Liquid Phase-Change Thermal Energy Storage Systems Through the Use of a High Conductivity Porous Metal Matrix, Ph.D. Dissertation, University of Idaho.
[17] Martin, B.W., (1967) Free convection in a vertical cylinder with internal heat generation, Proc. Roy. Soc. B, 301, pp. 327-341.
[18] El-Genk, M., and A.W. Cronenberg, (1978) “An Assessment of Fuel Freezing and Drainage Phenomena in a Reactor Shield Plug Following a Core Disruptive Accident,” Nuclear Eng. Design, 47, pp. 195-225.